BIOCHEMISTRY
including biophysical chemistry & molecular biology

Article

pubs.acs.org/biochemistry

Decrypting the Structural, Dynamic, and Energetic Basis of a Monomeric Kinesin Interacting with a Tubulin Dimer in Three ATPase States by All-Atom Molecular Dynamics Simulation

Srirupa Chakraborty and Wenjun Zheng*

Physics Department, University at Buffalo, Buffalo, New York 14260, United States

Supporting Information

ABSTRACT: We have employed molecular dynamics (MD) simulation to investigate, with atomic details, the structural dynamics and energetics of three major ATPase states (ADP, APO, and ATP state) of a human kinesin-1 monomer in complex with a tubulin dimer. Starting from a recently solved crystal structure of ATP-like kinesin−tubulin complex by the Knossow lab, we have used flexible fitting of cryo-electron-microscopy maps to construct new structural models of the kinesin−tubulin complex in APO and ATP state, and then conducted extensive MD simulations (total 400 ns for each state), followed by flexibility analysis, principal component analysis, hydrogen bond analysis, and binding free energy analysis. Our modeling and simulation have revealed key nucleotide-dependent changes in the structure and flexibility of the nucleotide-binding pocket (featuring a highly flexible and open switch I in APO state) and the tubulin-binding site, and allosterically coupled motions driving the APO to ATP transition. In addition, our binding free energy analysis has identified a set of key residues involved in kinesin−tubulin binding. On the basis of our simulation, we have attempted to address several outstanding issues in kinesin study, including the possible roles of β-sheet twist and neck linker docking in regulating nucleotide release and binding, the structural mechanism of ADP release, and possible extension and shortening of α4 helix during the ATPase cycle. This study has provided a comprehensive structural and dynamic picture of kinesin's major ATPase states, and offered promising targets for future mutational and functional studies to investigate the molecular mechanism of kinesin motors.

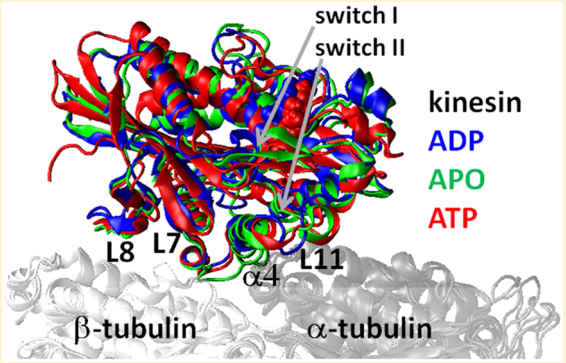

Kinesins, a prominent superfamily of molecular motors, utilize chemical energy from ATP hydrolysis to drive their unidirectional motion along microtubule (MT) filaments,[1] which are composed of repeating dimers of α- and β-tubulin.[2] Among 14 kinesin families, kinesin 1 was the first kinesin discovered,[3] and has been widely investigated as a model system for kinesin study. A full-length kinesin molecule consists of a catalytic core domain that harbors a nucleotide-binding pocket (involving three conserved nucleotide-binding motifs: switch I, switch II, and P loop)[4] and an MT-binding site,[5] a neck region as a mechanical amplifier,[6] a stalk domain for dimerization, and a tail domain for cargo binding. The main ATPase pathway of a kinesin monomer (in the presence of MT) has been extensively probed by kinetic studies,[7−11] which consists of the following key ATPase states: an ADP state where kinesin binds strongly with ADP and weakly with MT, an APO state where kinesin binds strongly with MT and weakly with nucleotide,[12] an ATP state where kinesin binds strongly with MT and generates force by docking its neck linker along the catalytic core domain,[6,13] an ADP-Pi state where kinesin binds with the products of ATP hydrolysis: ADP and inorganic phosphate (Pi). To fully understand the molecular mechanism of kinesin ATPase and motility, it is critical to investigate the above ATPase states and the transitions between them with high spatial and temporal resolutions.

The structural basis of kinesin's motor function remains elusive for the lack of detailed structural information for all ATPase states. Most high-resolution structures of kinesin were solved in the absence of tubulin.[14−16] So they cannot elucidate how MT binding activates the ATPase activities of kinesin (e.g., ADP release) and enables allosteric couplings between distant sites of kinesin.[17] Recently, the Knossow lab succeeded in solving a crystal structure of ATP-like kinesin−tubulin complex,[18] which shed new light on how strong binding between a kinesin and a tubulin dimer facilitates ATP hydrolysis and force generation. As an alternative to X-ray crystallography, cryo-electron microscopy (cryo-EM) has been utilized to image kinesin-decorated MT filaments.[19−24] It has enabled well-constrained fitting of kinesin and tubulin structures into cryo-EM maps (with subnanometer resolution), and identification of global and local structural changes between ADP, APO, and ATP state.[22] To fully utilize cryo-

Received: August 21, 2014
Revised: November 24, 2014
Published: December 23, 2014

DOI: 10.1021/bi501056h
Biochemistry 2015, 54, 859−869

EM data to constrain structural modeling, a number of flexible fitting techniques have been developed to optimize the fitting of a given initial protein structure with a cryo-EM map by exploiting protein structural flexibility.[25−33] For example, the molecular dynamics flexible fitting (MDFF) program steers individual protein atoms toward high-electron-density regions during a molecular dynamics (MD) simulation while preserving the correct stereochemistry and secondary structures.[34,35] There are still some open questions about the quality of cryo-EM-based flexible fitting: Do different techniques converge in modeling the kinesin−tubulin complex? Are those flexibly fitted models accurate enough to offer detailed insights to the structural mechanism of kinesin, especially the structural dynamics of kinesin−tubulin and kinesin-nucleotide interactions? It is important to address these issues before one can meaningfully interpret structural models constructed from subnanometer cryo-EM maps.

Structure-based computer simulation techniques, including coarse-grained modeling[36−43] and all-atom molecular simulation, have complemented experimental efforts to study the dynamic basis of kinesin's motor function. MD simulation[44] based on all-atom force fields[45] offers a powerful means to investigate protein dynamics and energetics in the presence of solvents and ions. Previously, all-atom MD simulations were performed to investigate the structural dynamics of various kinesins in the absence[46−53] or presence[52,54−56] of tubulin for up to tens of nanoseconds per trajectory (with the exception of ref 53, which performed 200 ns accelerated MD simulation of kinesin 5 in the absence of tubulin). However, these simulations were relatively short compared with the time scale of kinesin kinetics (∼ms). Thanks to fast improving computer hardware and software (e.g., graphics processing unit (GPU)-accelerated computer nodes and software[57]), it is now feasible to run longer (sub-μs) MD simulation for a large protein complex like the kinesin−tubulin complex.

In a previous study,[56] we conducted structural modeling for ADP, ATP, and APO state of a human kinesin-1 monomer bound with a tubulin dimer by flexible cryo-EM fitting, which is followed by short constrained MD simulation, hydrogen-bond analysis, and free energy calculation. The modeling and simulation revealed key nucleotide-dependent conformational changes between the above states, and dynamic hydrogen bonds at the nucleotide-binding pocket and the kinesin−tubulin interface.[56] However, two outstanding issues remain to be resolved: First, given the perturbation of cryo-EM-fitting forces and the shortness of constrained MD simulation (2 ns, see ref 56), it is uncertain if the cryo-EM-fitted models were adequately equilibrated and if they would still be stable in the absence of any constraint. Second, in ref 56 we modeled the strongly bound kinesin−tubulin complex starting from unbound kinesin and tubulin structures, which may require complex restructuring of the binding interface that is difficult to model reliably. In this study, we have addressed the above issues as follows: First, we have performed longer unconstrained MD simulations (total 400 ns per state), allowing for adequate equilibration of the system and meaningful analysis of the energetics and dynamics of kinesin in different ATPase states. Second, we have used a newly solved ATP-like structure of kinesin−tubulin complex[18] to model the strong-binding APO and ATP state, which allows more accurate modeling of the strong-binding kinesin−tubulin interface than the previous use of unbound structures.[56] Thanks to the above improvements, we have obtained a detailed structural and dynamic picture of kinesin's three major ATPase states, which has revealed nucleotide-dependent changes in the structure and flexibility of the nucleotide-binding pocket and the tubulin-binding site, and allosterically coupled motions driving the APO to ATP transition. Compared to our previous study,[56] we have also improved the analysis of key hydrogen bonds involved in kinesin-nucleotide and kinesin−tubulin interactions, and the calculation of the polar contribution to the kinesin−tubulin binding free energy. On the basis of the MD simulation, we will address the following outstanding questions in kinesin study: Is a twist of the central β-sheet involved in facilitating strong MT binding and ADP release? Is neck linker docking involved in the allosteric regulation of nucleotide binding? What is the structural and dynamic mechanism of MT-activated ADP release? Does the α4 helix undergo a nucleotide-dependent extension and shortening during the ATPase cycle?

METHODS

Initial Structural Modeling of Kinesin and Tubulin Dimer. We structurally modeled the following three ATPase states of a human kinesin-1 motor domain (referred as kinesin).

ADP State. A kinesin model was built on the basis of an ADP-bound kinesin 1 structure (PDB id: 1BG2, with neck linker truncated at residue 325).[58] To fit well with the cryo-EM map of ADP state,[22] the N-terminal segment of α4 helix (residues 247 to 256) was extended by the Modeller program[59] using a longer α4 helix of an ADP-bound kinesin 5 structure (PDB id: 1II6) as template (following ref 56). Residues 243 to 246 of loop L11 were remodeled accordingly by Modeller to link the extended α4 helix with the rest of loop L11 (residues 237 to 242). A tubulin dimer model was taken from an ATP-like structure of kinesin−tubulin complex (PDB id: 4HNA).[18]

ATP State. An ATP-like structure of kinesin−tubulin complex (PDB id: 4HNA)[18] was used as the initial model for ATP state and subject to flexible fitting of the ATP-state cryo-EM map (see below). The ATP analogue (i.e., ADP-AlF$_x$), together with Mg ion and two crystal waters at the active site of 4HNA, was kept for cryo-EM-based modeling and MD simulation (see below) to stabilize the closed nucleotide-binding pocket characteristic of ATP state.[60] We modeled two kinesin constructs: first with the neck linker (up to residue 337) in a docked conformation, second with the neck linker truncated at residue 325.

APO State. The ATP-like kinesin−tubulin structure (PDB id: 4HNA) was used as the initial model for APO state and subject to flexible fitting of the APO-state cryo-EM map (see below). The neck linker was truncated at residue 325 because it is disordered in the APO state. The ATP analogue, Mg ion and crystal waters at the active site of 4HNA were deleted.

In all three states, missing residues (residues 438−451 of α tubulin, 442−455 of β tubulin, 1−4 of kinesin) were added by the Modloop Web server,[61] except for residues 39 to 45 of α tubulin which were modeled by Modeller using the corresponding region of β tubulin as template. The protonation states of histidines were determined by the pK_a calculation using the PDB2PQR Web server (http://nbcr-222.ucsd.edu/pdb2pqr_1.9.0/).

Flexible Fitting of Cryo-EM Maps. For APO and ATP state, we rigidly fitted the initial model of kinesin−tubulin complex (see above) into the corresponding cryo-EM map of MT filaments decorated by nucleotide-free and ADP-AlF$_x$-bound kinesin using the Chimera program.[62] For ADP state, a sequential fitting function of Chimera was used to fit kinesin

DOI: 10.1021/bi501056h
Biochemistry 2015, 54, 859−869

and tubulin dimer separately as two rigid bodies while avoiding atomic clashes between them. The ligands (Mg and ADP or ADP-AlF$_x$) were included when fitting the cryo-EM maps of ADP or ATP state. Following rigid fitting, to further improve the fitting of electron densities and refine the kinesin−tubulin models, we performed flexible fitting with the MDFF program.[35]

Prior to running MDFF, we added hydrogen atoms with the VMD program.[63] Each kinesin−tubulin model was immersed into a rectangular box of water molecules extending to 12 Å from the protein periphery in x, y and z direction by VMD. To ensure an ionic concentration of 150 mM and zero net charge, Na^+ and Cl^- ions were added by VMD. Energy minimization of 2000 steps was performed using the steepest descent method to optimize the initial models under the constraint of cryo-EM maps.

We performed a 10 ns MDFF simulation using the NAMD program[64] and the CHARMM27 force field.[65] Water molecules were described by the TIP3P model.[66] The particle-mesh Ewald summation method[67] was used to evaluate long-range electrostatic forces with a grid size of <1 Å. An integration time step of 1 fs was used in the framework of a multiple time-stepping algorithm.[68] A 12-Å cutoff distance was used for nonbonded interactions, and a temperature of 300 K was maintained using the Langevin thermostat[69] which was coupled to all heavy atoms with a damping coefficient of 5.0 ps^{-1}.

MDFF adds two external potentials (U_{EM}, U_{SS}) to the usual MD potential,[34] where U_{EM} is derived from the gradient of electron density, and U_{SS} enforces harmonic restraints to preserve secondary structure elements such as α-helices and β-strands. The parameters for U_{EM} and U_{SS} were set to be $\xi = 0.3$ kcal mol^{-1} and $k_\mu = 300$ kcal mol^{-1} $Å^{-2}$, as recommended in ref 34. To gradually release the cryo-EM restraints and allow a smooth transition to subsequent unconstrained MD simulation (see below), ξ was lowered by 0.05 every 2 ns.

To assess the convergence of cryo-EM-fitted models by different flexible fitting methods (including MDFF), we fitted the APO-state cryo-EM map using two alternative methods: EMFF[32] (available via a Web server at http://enm.lobos.nih.gov/emff/start_emff.html) and Rosetta density fitting,[33] resulting in two alternative APO-state models of kinesin−tubulin complex to be compared with the MDFF-generated models.

Equilibrium MD Simulation. Following 8 ns MDFF simulation, we continued with regular MD simulation of 100 ns without the cryo-EM restraint at constant temperature and pressure. During the MD simulation, to stabilize the tubulin dimer structure while allowing for full flexibility of kinesin and kinesin−tubulin interface, we restrained the Cα atoms of tubulin residues which are greater than 12 Å away from kinesin by harmonic springs with force constant of 1 kcal mol^{-1} $Å^{-2}$. Four independent MD simulations were conducted following four MDFF runs, resulting in total 400 ns MD trajectories for each state. The Nose−Hoover method[70] was used with temperature T = 300 K and pressure P = 1 atm. Periodic boundary conditions were applied to the system. A 10-Å switching distance and a 12-Å cutoff distance were used for nonbonded interactions. The SHAKE algorithm was used to constrain bond lengths of hydrogen-containing bonds, which allowed a time step of 2 fs for MD simulation. The snapshots of the system were saved every 20 ps during MD simulation for later analysis (see below), resulting in 5000 snapshots per trajectory. The MD simulation was conducted with the NAMD program[64] using the CHARMM27 force field.[65]

RMSF Analysis. To assess the local flexibility of kinesin residues in ADP, APO, and ATP state based on MD simulation, we calculated the root mean squared fluctuation (RMSF) as follows: first, we saved 4 × 2500 snapshots of the kinesin−tubulin complex during the last 50 ns of four MD trajectories in each state; second, we superimposed the C_α coordinates of kinesin alone or kinesin−tubulin complex (excluding the floppy C-terminal loops of $\alpha\beta$-tubulin) with minimal root mean squared deviation (RMSD); finally, we calculated the following RMSF at residue position n:

$$\mathrm{RMSF}_n = \sqrt{\frac{1}{M}\sum_{m=1}^{M} |\vec{r}_{mn} - \langle \vec{r}_n \rangle|^2} \quad (1)$$

where $\vec{r}_{mn}$ is the C_α atomic position of residue n in snapshot m, $\langle \vec{r}_n \rangle = (1/M)\sum_{m=1}^{M} \vec{r}_{mn}$ is the average C_α atomic position of residue n, and M = 10000 is the total number of snapshots.

Principal Component Analysis (PCA). To identify dominant modes of structural fluctuations in the kinesin−tubulin complex during MD simulation, we performed the principal component analysis (PCA) as follows: first, we saved 4 × 2500 snapshots of the last 50 ns of four MD trajectories in each state; second, we superimposed the C_α coordinates of kinesin−tubulin complex (excluding the floppy C-terminal loops of $\alpha\beta$-tubulin) with minimal RMSD; third, we calculated a covariance matrix comprised of the following 3 × 3 blocks

$$C_{nn'} = \frac{1}{M}\sum_{m=1}^{M} (\vec{r}_{mn} - \langle \vec{r}_n \rangle) \otimes (\vec{r}_{mn'} - \langle \vec{r}_{n'} \rangle) \quad (2)$$

fourth, we diagonalized the covariance matrix and kept two modes with the highest eigenvalue. Here the eigenvalue of each mode gives the contribution of that mode to the total structural fluctuations, and the eigenvector of each mode describes a specific conformational change sampled during MD simulation.

Calculation and Partition of Kinesin−Tubulin Binding Free Energy. Following our previous paper,[55,56] we calculated the kinesin−tubulin binding free energy ΔG in ADP, ATP, and APO state. We extracted 10000 snapshots of the last 50 ns of four MD trajectories in each state. For each snapshot, we calculated ΔG using a continuum solvent model (see ref 71), which expresses ΔG as $\Delta G_{np} + \Delta G_{elec}$. Here the nonpolar contribution $\Delta G_{np} = \alpha E_{vdW}$ was empirically written as a fraction ($\alpha < 1$) of the van der Waals (vdW) interaction energy E_{vdW} between kinesin and tubulin dimer, and the electrostatic contribution $\Delta G_{elec} = \beta \Delta E_{elec}$ was written as a fraction ($\beta < 1$) of the change in electrostatic energy ΔE_{elec} from unbound kinesin and tubulin to kinesin−tubulin complex. E_{elec} was calculated using the Poisson−Boltzmann (PB) method[72,73] (for details, see ref 55). α = 0.158 and β = 0.153 were calibrated using mutational data in our previous paper.[55] Because of the high uncertainty in entropy calculation, we did not include the entropic contribution to ΔG, which resulted in a negative shift of ΔG by 7−15 kcal/mol relative to true ΔG.[46]

Next, we used the CHARMM program[74] to partition ΔG, E_{vdW}, and ΔE_{elec} to contributions from individual kinesin residues (denoted ΔG_n, $E_{vdW,n}$ and $\Delta E_{elec,n}$ for residue n, for details see analys.doc and pbeq.doc at http://www.charmm.org/documentation/c37b1/index.html). Then we ranked all kinesin residues by ΔG_n and kept the top 5%, which were predicted to be important to kinesin−tubulin binding. The

DOI: 10.1021/bi501056h
Biochemistry 2015, 54, 859−869

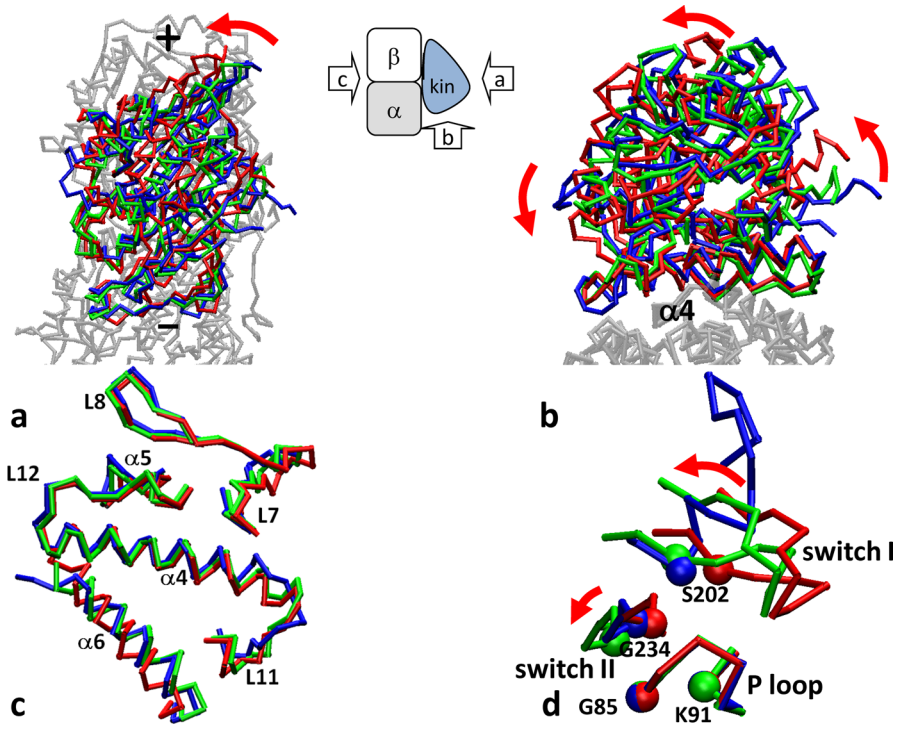

Figure 1. Conformational changes between flexibly fitted models of kinesin−tubulin complex in ADP, APO, and ATP state: (a) top view of a rotation of kinesin relative to tubulin (from ADP and APO state to ATP state, indicated by a red arrow); (b) side view of a seesaw rotation of kinesin relative to tubulin (from ADP and APO state to ATP state, indicated by red arrows); (c) bottom view (with tubulin dimer removed) of movements of tubulin-binding motifs in kinesin (including loop L7, L8, L11, L12, and α4, α5, α6 helix as labeled); (d) movements of switch I and II in the nucleotide-binding pocket (with P loop as reference and key residues shown as spheres and labeled). Models of ADP, APO, and ATP state are colored blue, green, and red, respectively. The viewing directions of panels (a)−(c) are shown in a cartoon inset.

choice of 5% corresponds to a p value of 0.05 (i.e., the probability that a random ranking of all kinesin residues places a given residue in the top 5%), which is widely used as the standard significance level.

RESULTS AND DISCUSSION

Initial Structural Modeling of ADP, ATP, and APO State of Kinesin. We have revisited structural modeling of ADP, ATP, and APO state of human kinesin 1 after the recent publication of a new ATP-like structure of kinesin−tubulin complex (PDB id: 4HNA).[18] Compared with our previous work,[56] the following changes and improvements were made in the new modeling:

For ADP state, we followed a similar modeling procedure for kinesin that started from an ADP-bound crystal structure of kinesin 1 (PDB id: 1BG2), and then extended the α4 helix by 2 turns with homology modeling to fit the cryo-EM densities of α4 helix[22] (see Methods). Unlike ref 56 we used a different model of tubulin dimer from ref 18 to be consistent with the modeling of ATP and APO state (see below).

For ATP state, we directly used the new ATP-like structure of kinesin−tubulin complex from ref 18 which captured ATP-like structural features (such as closed nucleotide-binding pocket, docked neck linker and strong-binding kinesin−tubulin interface). Here the ATP state is defined as the state visited after ATP-binding isomerization and before ATP hydrolysis, which corresponds to experimental structures of kinesin bound with ADP-AlF$_x$ (AlF$_x$ is an analogue of γ-phosphate of ATP) and tubulin/MT in the literature.[18,22]

For APO state, we also used the new ATP-like structure of kinesin−tubulin complex from ref 18 because it captured the strong-binding kinesin−tubulin interface better than those unbound kinesin structures used previously.[56] This approximation is necessary because no nucleotide-free crystal structure of kinesin is available to date (kinesin is structurally unstable in the absence of nucleotide and MT[75]). Extensive conformational changes are expected to transform this initial model to a final model for APO state through flexible fitting of an APO-state cryo-EM map (see below).

Rigid and Flexible Fitting of Cryo-EM Maps in ADP, ATP, and APO State. In a previous study, Sindelar and Downing solved three cryo-EM maps of kinesin-1-decorated MT filaments in the presence of ADP, ADP-AlF$_x$, and in the absence of nucleotide, which correspond to ADP, ATP, and APO state, respectively.[22] The subnanometer resolution (~8.9 Å) allowed them to place atomic structures of unbound kinesin and tubulin dimer readily into the maps, and detect subtle discrepancies (e.g., in the nucleotide-binding pocket and kinesin-MT interface) between unbound structures and cryo-EM densities indicative of conformational changes induced by kinesin-MT binding.[22] Cryo-EM maps with similar resolution were obtained for kinesin 5 as well.[23,24] These cryo-EM maps offer useful constraints for accurate modeling of a kinesin−tubulin complex in different ATPase states. To this end, we have performed rigid and flexible fitting of cryo-EM maps using the kinesin and tubulin dimer models described in the previous section. First, we used rigid cryo-EM fitting to construct an initial model of kinesin−tubulin complex in ADP, APO, and ATP state (see Methods). Second, we employed the MDFF program[34,35] to flexibly fit the initial kinesin−tubulin model into the corresponding cryo-EM map in ADP, APO, and ATP state.[22] We performed four independent MDFF simulations for

DOI: 10.1021/bi501056h
Biochemistry 2015, 54, 859−869

each state. Unlike our previous study,[56] we ran longer (10 ns) MDFF simulations with gradually decreasing cryo-EM-fitting forces, which would reduce structural perturbation by cryo-EM fitting and allow a smooth transition to subsequent unconstrained MD simulation (see below).

To evaluate fitting quality, we calculated the local cross-correlation coefficient (CCC) for electron densities within 8.9 Å of the molecular surface of kinesin−tubulin complex. We found MDFF indeed improved the fitting of the cryo-EM maps over rigid fitting (see Figure S1). The CCC values were improved from 0.65 to 0.72 in ADP state, from 0.67 to 0.79 in APO state, and from 0.80 to 0.86 in ATP state. The CCC values for new MDFF-fitted models were comparable to the old models from ref 56 (CCC ∼0.78 in ADP state, ∼0.81 in APO state, and ∼0.79 in ATP state). Notably, the new ATP-state models fit better than the old models from ref 56, supporting the advantage of using the new ATP-like structure of kinesin−tubulin complex.[18]

During MDFF simulation, the largest conformational changes were observed in APO state (RMSD ∼ 3.5 Å) among the three states. Indeed, extensive conformational changes are required to transform the initial ATP-like structure to the final APO-state structure, which involve a clockwise rotation of kinesin on top of tubulin dimer (see Figure S1(b)), and restructuring of the tubulin-binding interface (see Figure S2(a)) and the nucleotide-binding pocket (see Figure S2(b)). Can flexible cryo-EM fitting reliably model such complex conformational changes? To answer this question, we assessed how well the flexibly fitted models of APO state converge between different MDFF runs and between MDFF and two alternative flexible fitting methods (i.e., EMFF[32] and Rosetta density fitting[33]). The four independent MDFF runs generated very similar models of APO state (RMSD ≤ 1 Å between each MDFF model and the average structure of four MDFF models). The alternative models generated by EMFF and Rosetta were also fairly similar to the MDFF models (RMSD ≤ 1.9 Å relative to the average structure of four MDFF models). The three flexible fitting methods predicted similar conformational changes at the tubulin-binding interface (e.g., in α4 helix, α6 helix, loop L11, and loop L12, see Figure S2(a)) and the nucleotide-binding pocket (e.g., in switch I and II, see Figure S2(b)). Therefore, the subnanometer cryo-EM maps indeed offer sufficient constraints to enable robust structural modeling of the kinesin−tubulin complex by flexible fitting.

Analysis of Conformational Changes between ADP, APO, and ATP State. Following the flexible cryo-EM fitting, we compared the kinesin−tubulin models in three ATPase states (ADP, APO, and ATP state) to reveal conformational changes accompanying key ATPase events of kinesin (ADP release and ATP binding). We observed large global conformational changes between ADP/APO and ATP state, featuring a counterclockwise rotation of kinesin on top of tubulin (see Figure 1(a)), and a seesaw-like rotation of kinesin as viewed along the MT axis (see Figure 1(b)). These rotations were also observed in previous cryo-EM studies of kinesin 1[22] and kinesin 5.[23] We did not observe a tilting of kinesin toward MT from ADP to APO state as found in a recent cryo-EM study of kinesin 5.[24]

Next we focused on the structural changes at the kinesin−tubulin interface and the nucleotide-binding pocket.

Structural Changes at the Kinesin−Tubulin Interface (see Figure 1(c)). We superimposed the MDFF-generated kinesin−tubulin models in three ATPase states along the tubulin dimer. We found loop L7 moves closer to tubulin in APO and ATP state than ADP state, supporting its role in sensing and facilitating strong MT binding.[76] We found loop L8 barely moves between these states, supporting its role as an anchor point of kinesin on tubulin in all three states.[15] Similar to L8, we found α4 helix's position and orientation roughly fixed in all three states,[22,23] except for slight bending of its C-terminal region and adjacent loop L12 closer to tubulin in APO state than ADP and ATP state. We found the N-terminal region of loop L11 moves closer to tubulin in APO and ATP state than ADP state, supporting its role in enabling strong MT binding.[14] α6 helix was found to adopt different orientations between ATP state and the other two states to accommodate distinct neck linker conformations (i.e., docked in ATP state and undocked in the other states).

Local Structural Changes at the Nucleotide-Binding Pocket (see Figure 1(d)). To explore nucleotide-dependent structural changes of switch I and II relative to P loop, we superimposed the MDFF-generated kinesin models of three ATPase states along P loop. The switch-I structure features a short helical form distant from P loop in ADP state, and an extended form close to P loop in APO and ATP state (as observed in a recent cryo-EM study[24]). We found switch I undergoes a large open-to-close movement from ADP state to APO state and then ATP state. In APO state, switch I adopts an intermediate position between the open position of ADP state and the closed position of ATP state, whereas switch II adopts a more open position than ADP and ATP state. This is consistent with the proposal that a fully open switch II enables complete release of Mg and ADP.[77] We should caution that the *static* conformations of switch I and II determined by cryo-EM fitting cannot represent ensemble of *dynamic* conformations sampled by switch I and II under physiological conditions. Indeed, in ref 56, we found switch I to be structurally flexible and undetermined by cryo-EM densities in APO state. There was also strong evidence for considerable variations in switch I among kinesin crystal structures.[78] To address this issue, we have analyzed the dynamic fluctuations of the nucleotide-binding pocket (involving key residues of P loop, switch I, and switch II) based on MD simulations of these states (see below and Supporting Information).

MD Simulations of ADP, APO, and ATP State. Although providing structural snapshots of key ATPase states, the MDFF-generated models of kinesin−tubulin complex are subject to perturbation of cryo-EM-fitting forces, and influence of the initial models used for fitting (e.g., the cryo-EM-fitted models of APO state might retain some residual ATP-like features from the initial model). To further relax the cryo-EM-fitted models and explore the dynamic behaviors of kinesin interacting with tubulin dimer under physiological conditions, we performed four independent 100 ns-long MD simulations of kinesin−tubulin complex in the presence of solvents and ions starting from the MDFF-generated models of ADP, APO, and ATP state (see Methods).

To assess the conformational stability of our MD simulation, we calculated the RMSD for C_α atoms relative to the starting models (see Figure S3). For all MD trajectories, the system stabilized within <50 ns as indicted by saturating RMSD ∼2 Å. So we kept 5000 snapshots of the last 50 ns of four MD trajectories in each state, and combined them to construct a structural ensemble for each state for later analysis (see below). We also checked the robustness of our MD-based calculations by repeating the analysis for the last 25 ns of MD trajectories to

DOI: 10.1021/bi501056h
Biochemistry 2015, 54, 859−869

ensure the results are not sensitive to the truncation of MD trajectories.

To further assess the stability of the binding interface between kinesin and tubulin dimer during MD simulation, we calculated the kinesin–tubulin contact surface area (CSA) for four MD trajectories in ADP, APO, and ATP state (see Figure S4). The CSA was calculated as half the difference between the solvent accessible surface areas of unbound proteins and the bound complex using the SASA program.[79] Although the CSA values are highly fluctuating (especially in ADP state, see Table S1), we found no sign of CSA decreasing during the course of MD simulation, suggesting no destabilization of the kinesin–tubulin interface during MD simulation. As expected, the CSA values are significantly higher in APO and ATP state than ADP state (see Table S1), which is consistent with stronger MT binding in APO and ATP state than ADP state.

Flexibility Analysis of Kinesin Residues in ADP, APO, and ATP State. On the basis of the MD simulation in three ATPase states, we calculated root mean squared fluctuation (RMSF) which measures the amplitude of fluctuation of individual kinesin residues with respect to an average kinesin–tubulin structure (see Methods and Figure 2(a)). To focus on fluctuations within kinesin, we also calculated RMSF with respect to an average structure of kinesin alone (see Figure 2(b)). Overall, kinesin is more flexible in ADP state than APO and ATP state (see Figure 2(a)), which is mainly due to larger mobility of a weakly bound kinesin relative to tubulin dimer in ADP state.[80] Indeed, the three states are comparable in overall flexibility within kinesin (see Figure 2(b)). This is in contrast to the finding in ref 53 that kinesin is more flexible in APO state than ADP and ATP state in the absence of tubulin. This finding supports the importance of tubulin binding in dictating the dynamics of kinesin (especially in APO state).

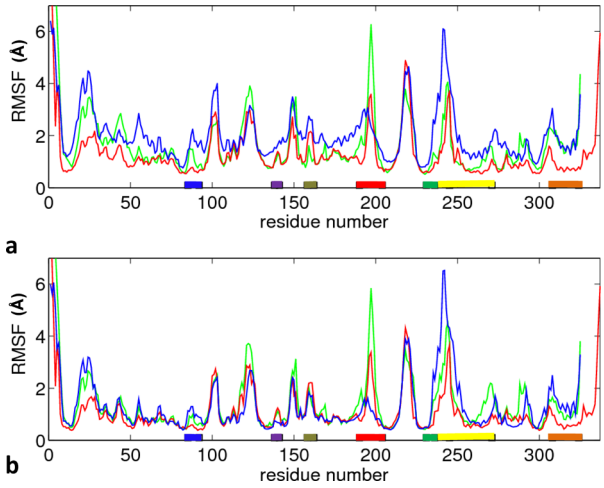

Figure 2. Results of RMSF analysis for structural fluctuations of kinesin residues: (a) with respect to an average kinesin–tubulin structure; (b) with respect to an average kinesin structure. RMSF curves of ADP, APO, and ATP state are colored blue, green, and red, respectively. Key kinesin motifs are marked and colored as follows: P loop (blue), switch I (red), switch II (green), loop L7 (purple), loop L8 (tan), loop L11 and α4 helix (yellow), and α6 helix (orange).

On the basis of the RMSF calculation, we further analyzed nucleotide-dependent changes in local flexibility of the following key kinesin sites:

At the nucleotide-binding pocket, switch I is more flexible in APO state than ATP and ADP state (see Figure 2), which may dynamically open the pocket to allow rapid release of nucleotide in APO state. In contrast, switch II (together with adjacent loop L11) is more flexible in ADP state than ATP and APO state (see Figure 2), which may be due to less stabilization by weaker tubulin binding in ADP state than ATP and APO state. A disordered switch II in ADP state was observed in a recent cryo-EM study of kinesin 5.[24] The above flexibility analysis provided a dynamic picture of the opening/closing of nucleotide-binding pocket which complements the static view of structural differences in nucleotide-binding pocket between three ATPase states (see Figure 1(d)).

At the tubulin-binding interface (e.g., loop L7, L8, L11, and α4 helix), ADP state exhibits higher flexibility than APO and ATP state (see Figure 2a), which is consistent with weak MT binding in ADP state. Loop L11 is flexible even in APO and ATP state (see Figure 2). The functional importance of L11 flexibility was highlighted by a S to G substitution in residue position 239 of a fast fungal kinesin.[81] α6 helix is more flexible in APO and ADP state than ATP state (see Figure 2), which is consistent with distinct neck-linker conformations in these states (i.e., disordered in APO and ADP state, and docked in ATP state).

To test the proposal that the N-terminal region of α4 helix undergoes nucleotide-dependent extension and shortening,[14,16,82] we compared RMSF in this region between three ATPase states, and found similar RMSF distribution with comparable flexibility in APO and ATP state (see Figure 2(b)). We also visualized the MD simulation of tubulin-binding interface in ADP, APO, and ATP state (see Movie S1), and found α4 helix to be structurally stable except for transient unwinding of one turn at the N-terminus. Therefore, our simulation does not support a significant change in the length of α4 helix as observed by structural studies of kinesin in the absence of tubulin,[14,16,82] while it is in agreement with two cryo-EM studies of kinesin-decorated MT filaments.[22,23]

Analysis of the Twist of Central β-Sheet in Kinesin in Comparison with Myosin. To test the proposal that a twist of central β-sheet facilitates strong MT binding and ADP release in kinesin,[77,83] we have analyzed the twist of β-sheet in the MDFF and MD simulation of ADP, APO, and ATP state (see Table S2), in comparison with crystal structures of kinesin and myosin (see Table S3). We calculated a twist angle between strand β1 (represented as a vector pointing from residue K10 to R14) and β4 (represented as a vector pointing from residue V132 to E136) which are structurally conserved between kinesin and myosin (see Figure S5).

For crystal structures of myosin classified into three states (ADP-Pi state, ATP state, and APO state), the twist angle increases by up to 25° in the order of ADP-Pi < ATP < APO (see Table S3). In comparison, for crystal structures of kinesin classified into two states (ATP-like and ADP-like state), the twist angle increases by <10° from ATP-like to ADP-like state (see Table S3). Similar order was found in our MD simulation: the twist angle increases from 63.8 ± 2.5° in ATP state to 68.3 ± 3.5° in ADP state (see Table S2). Interestingly, the APO state showed a greater twist (70.6 ± 3.2°) than both ADP and ATP state (see Table S2), which is even greater than the maximum twist angle (~69°, see Table S3) observed in a KIF14 crystal structure.[84] This finding supports the proposed role of β-sheet twist in strong MT binding of kinesin akin to myosin.[77,83] Compared with the MD simulation, the MDFF-

DOI: 10.1021/bi501056h
Biochemistry 2015, 54, 859–869

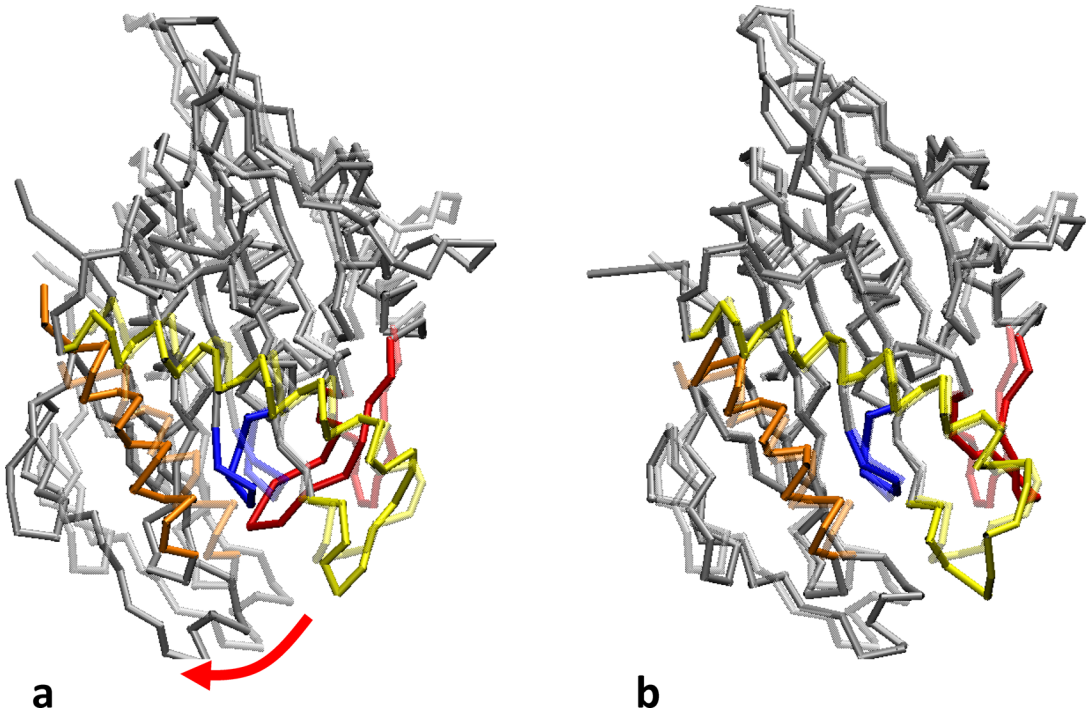

Figure 3. Conformational changes in kinesin predicted by the following PCA modes in APO state: (a) mode 1 (b) mode 2. Kinesin structure before and after the predicted conformational changes are shown as transparent and opaque, respectively. Key kinesin motifs are colored as follows: P loop (blue), switch I (red), loop L11 and α4 helix (yellow), and α6 helix (orange). In panel (a), a global rotation of kinesin is indicated by a red arrow.

generated models showed less twist in β-sheet (see Table S2), suggesting the importance of dynamic fluctuations in driving the β-sheet twist in kinesin.

Notably, the fourth MD trajectory in ADP state showed an unusually high twist angle (72.3 ± 2.7°). A detailed analysis of this trajectory revealed a larger kinesin−tubulin contact surface area (see Table S1) and a more open switch I at the nucleotide-binding pocket (see Table S4). This preliminary finding is consistent with the proposed role of central β-sheet twist in MT-binding-activated ADP release.[77,83]

Analysis of Allosterically Coupled Motions in MD Simulation of APO State. It is generally believed that allosteric couplings between the nucleotide-binding pocket, the MT-binding site, and neck linker facilitate the ATPase-driven motility of kinesin, and such couplings require the presence of MT binding. Toward elucidating the structural and dynamic basis of such allosteric couplings, principal component analysis (PCA) was previously employed to derive major conformational changes among various kinesin crystal structures.[53,85] However, the usefulness of such analysis was limited by the lack of tubulin binding in these structures. Thanks to our extensive MD simulation of the kinesin−tubulin complex in three ATPase states, we are now able to address this outstanding issue. To this end, we performed PCA on the MD-generated structural ensemble of APO state (see Methods) to identify dominant modes of structural fluctuations which may allosterically couple distant sites of kinesin and initiate conformational transitions between different ATPase states.

We focused on two dominant PCA modes which accounted for 32% and 18% of overall structural fluctuations, respectively.

Mode 1 predicts extensive global and local conformational changes, including a clockwise rotation of kinesin with α4 helix roughly anchored on tubulin dimer, a reorientation of α6 helix to allow docking of neck linker, closing of switch I relative to P loop, and a movement of loop L11 toward the nucleotide-binding site (see Figure 3(a)). Interestingly, all these conformational changes are involved in the conformational transition from APO to ATP state, suggesting that our extensive MD simulation in APO state was able to sample conformational space in the direction of ATP state even in the absence of ATP binding.

Mode 2 predicts primarily local conformational changes, including opening of switch I relative to P loop and a movement of loop L11 toward tubulin (see Figure 3(b)). Similar local conformational changes were also observed in the PCA of ADP state (data not shown), which may allow MT binding to trigger opening of the nucleotide-binding pocket to allow ADP release. This finding supports the proposed role of switch I displacement in stimulating MgADP release.[81]

In sum, our PCA based on the APO-state MD simulation revealed large global and local structural fluctuations that initiate the conformational transition toward ATP state, and shed light on how MT binding facilitates opening of the nucleotide-binding pocket to allow ADP release. The dominant PCA modes revealed high flexibility of switch I in APO state in agreement with the analysis of RMSF (see Figure 2) and dynamics of the nucleotide-binding pocket (see Results and Table S4 in Supporting Information).

Calculation and Partition of Binding Free Energy in ADP, APO, and ATP State. As evident from biochemical measurements,[9,17] kinesin binds MT weakly in ADP state, and strongly in APO and ATP state. Such difference in MT-binding affinity is essential to drive structural changes that release ADP, facilitate ATP binding and hydrolysis, and generate force. In our previous studies,[55,56] we established and applied an MD-based binding free energy calculation protocol (see Methods) to the kinesin−tubulin complex which yielded lower (more negative) binding free energy (denoted ΔG) for APO and ATP

DOI: 10.1021/bi501056h
Biochemistry 2015, 54, 859−869

state than ADP state. Here we recalculated ΔG based on the new kinesin−tubulin models and more extensive MD simulations. The new ΔG value of APO or ATP state is similar to the old value from ref 56, while ΔG is higher (less negative) for ADP state (see Table S6). This is because the unrestrained kinesin is more mobile during the new longer MD simulation of ADP state, so it can move further away from tubulin dimer, resulting in weaker binding. Nevertheless, the higher mobility of kinesin also entails more favorable entropy (not considered in our calculation) which partially compensates the unfavorable binding energy. Next, we did a breakdown of ΔG into electrostatic (polar) and van der Waals (nonpolar) contribution. The nonpolar contribution follows the order of ADP < ATP ≤ APO, which correlates well with ΔG (see Table S6) and the kinesin−tubulin contact surface area (see Table S1), supporting the importance of van der Waals contact forces to kinesin−tubulin binding. Interestingly, the polar contribution follows a similar order of ADP < APO ≤ ATP, which explains why the hydrogen bond (HB) analysis was found useful in distinguishing between weak and strong MT-binding states, and identifying key residues involved in kinesin−tubulin binding (see Supporting Information).

Next, to identify those residues important to kinesin−tubulin binding, we partitioned ΔG to individual kinesin residues (see Methods and ref 86). We kept top 5% kinesin residues for each state (see Table S7). As expected, they are distributed over known MT-binding motifs including loop L2 (K44), L7 (K141), L8 (K159, R161, and K166), L11 (K237, V238, S239, K240, and L248), L12 (Y274 and R278), α4 (K252, N255, K256, and N263), α5 (K281 and R284), and α6 helix (K313 and R321). Most of them are positively charged residues with a few polar (S239, N255, and N263) and nonpolar residues (V238, L248, and Y274), which highlights the importance of extensive electrostatic interactions and local nonpolar interactions to kinesin−tubulin binding. Many of them were also identified by the HB analysis (see Supporting Information). Some of them contribute more to the strong MT-binding APO and ATP state than the weak MT-binding ADP state (such as K159, K237, V238, S239, K240, L248, K252, N255, K256, Y274, R278, K281, and R284). This finding offers a list of promising target residues for future mutational and functional study of kinesin-MT binding during the ATPase cycle of kinesin.

Relating Our Simulation to Open Issues in Kinesin Study. Our simulation allows us to address a number of outstanding issues and controversies important to the elucidation of kinesin function, which are discussed as follows.

Twist of the Central β-Sheet. Recent structural studies of myosin (a superfamily of molecular motors evolutionarily related to kinesin) revealed a twist of its central β-sheet in the rigor-like conformation (corresponding to APO state) that closes the actin-binding cleft and opens the nucleotide-binding pocket to allow Pi and ADP release.[87,88] This finding inspired a speculation that kinesin may undergo a similar twist of its central β-sheet to enable strong MT binding[83] and MT-activated ADP release.[77] In support of this proposal, a large change in the central β-sheet was observed by a cryo-EM study of a kinesin 14 motor,[20] and a large twist of the central β-sheet was found in a new crystal structure of ADP-bound KIF14.[84] However, no such twist was observed in other cryo-EM studies of nucleotide-free kinesin 1[22] and kinesin 5.[23] The first computational evidence for a nucleotide-dependent twist of the β-sheet was found in a recent MD simulation study of KIF1A (a member of the kinesin 3 family).[52] To address the above controversy, we have analyzed the angle of twist in the central β-sheet of kinesin 1 during the MD simulation in ADP, APO, and ATP state in comparison with various crystal structures of kinesin and myosin (see Table S2 and S3). Our simulation demonstrated a more twisted β-sheet in APO state than ADP and ADP state, although it is significantly smaller than myosin. Interestingly, one of our ADP-state simulations indicated a correlation of the β-sheet twist (see Table S2) with opening of switch I (see Table S4) and stronger kinesin−tubulin binding (see Table S1 and S6), thus supporting the proposed role of β-sheet twist in enabling strong MT binding[83] and ADP release.[77] The nucleotide-dependent twist of the β-sheet as found in our MD simulation differs from that observed in the MD simulation of KIF1A[52] (see Results and Table S8 in Supporting Information).

Stability of α4 Helix. On the basis of a recent structural study of a KIF4 motor[82] in comparison with previous structures of KIF4,[14−16] it was proposed that the length of α4 helix (and adjacent loop L11) undergoes a nucleotide-dependent change during the ATPase cycle of kinesin which couples to changes in the kinesin-MT binding affinity and the nucleotide-binding pocket. However, two cryo-EM studies[22,23] found no extension or shortening of α4 helix during the ATPase cycle of kinesin 1 and 5, while one cryo-EM study found melting of α4 helix in a nucleotide-free kinesin 14 motor.[20] To address the above controversy, we analyzed the structural flexibility of α4 helix during the MD simulation of ADP, APO, and ATP state (see Figure 2), and we found α4 helix to be structurally stable in all three states (except for partial unwinding of one turn at the N-terminus, see Movie S1), which could be attributed to the stabilization effect of tubulin binding.

Regulation of Nucleotide Binding by Neck Linker Docking. Previous structural and kinetic studies supported a role of neck linker docking in allosteric regulation of nucleotide binding.[89,90] To probe the structural and dynamic basis of this regulation, we have run and compared MD simulation for two kinesin constructs in ATP state (one with a docked neck linker and the other with the neck linker truncated). Interestingly, we found a more flexible and open switch I in the latter construct (see Results and Table S4 in Supporting Information), which suggests that a docked neck linker may regulate nucleotide binding by allosterically stabilizing a closed nucleotide-binding pocket.

MT-Activated ADP Release. Our MD simulation of ADP and APO state has offered new insights to the structural and dynamic mechanism of MT-activated ADP release. Our finding of an open and highly flexible switch I in APO and ADP state (see Table S4 and Figure 2) substantiates the proposal that MT-induced switch-I displacement stimulates the release of MgADP.[91] In addition, our simulation predicts a more open switch II in APO state than ADP state (see Table S4 and Figure 1(d)), which may further destabilize MgADP coordination by switch II.[78,92] Together, the movements of both switch I and II may contribute to MT-activated ADP release.

Comparison of This Study with Our Previous Study.[56] Despite predicting similar nucleotide-dependent conformational changes (see Figure 1 of this study vs Figure 2 and Figure 3(a) of ref 56), the new models and simulations of kinesin−tubulin complex have shown the following improvements over ref 56:

(1) The new ATP-state models generated by MDFF fit better with the cryo-EM map than the old models from ref 56,

DOI: 10.1021/bi501056h
Biochemistry 2015, 54, 859−869

which may be attributed to the use of the new ATP-like structure of kinesin−tubulin complex.[18]

(2) In the old ATP-state models from ref 56, loop L8 was shifted away from tubulin compared with the other states. In the new models, we found loop L8 barely moves between these states, which is consistent with the finding of L8 as an anchor point of kinesin on tubulin in all three states by a previous cryo-EM study[15] and mutational study.[14]

(3) As revealed by the HB analysis (see Results and Table S5 of Supporting Information), our new modeling and simulation of ATP state led to an improved description of the closed nucleotide-binding pocket with more high-occupancy HBs formed between the nucleotide-binding motifs and AlF_x.

(4) As revealed by the HB analysis, we found significant differences in the total counts of kinesin−tubulin HBs compared with ref 56. We found fewer HBs in ADP state, and more HBs in APO and ATP state than ref 56. As a result, the new HB counts are consistent with weak (strong) MT binding in ADP state (APO and ATP state), while the old HB counts in ref 56 are not. The above differences may be due to the use of unconstrained MD simulations that allow more HBs to break in ADP state, and the discrepancy in the conformation of loop L8 in ATP state (see above).

(5) In the analysis of kinesin−tubulin binding free energy, the new ADP state exhibited weaker binding than in ref 56. This difference is probably due to the use of long unconstrained MD simulation here vs short constrained MD simulation in ref 56. Here we found the polar contribution to ΔG follows an order of ADP < APO $\leq$ ATP similar to the nonpolar contribution, while ref 56 found a different order: ATP < APO < ADP. The above difference in the polar interactions between kinesin and tubulin is related to the finding of different counts of kinesin−tubulin HBs as discussed above.

■ ASSOCIATED CONTENT

Supporting Information

Methods on hydrogen-bond analysis. Results on the analysis of opening/closing of the nucleotide-binding pocket and hydrogen bonds in ADP, APO, and ATP state. **Figure S1**. Visualization of kinesin−tubulin models rigidly or flexibly fitted into a cryo-EM map in APO state. **Figure S2**. Comparison of APO-state kinesin−tubulin models built by rigid fitting and three flexible fitting methods. **Figure S3**. Root mean squared deviation as a function of time for four MD trajectories. **Figure S4**. Kinesin−tubulin contact surface area as a function of time for four MD trajectories. **Figure S5**. The central β-sheet of an ATP-like kinesin structure. **Figure S6**. Selected hydrogen bonds formed in ADP, APO, and ATP state. **Table S1**. The kinesin−tubulin contact surface area calculated on the basis of four MD trajectories in ADP, APO, and ATP state. **Table S2**. The twist angle of central β-sheet calculated on the basis of four MDFF-generated models and four MD trajectories in ADP, APO, and ATP state. **Table S3**. The twist angle of central β-sheet calculated for crystal structures of myosin and kinesin. **Table S4**. Key atomic distances in the nucleotide-binding pocket calculated on the basis of four MD trajectories in ADP, APO, and ATP state in comparison with MDFF-generated models. **Table S5**. Results of hydrogen bond analysis based on MD simulation in ADP, APO, and ATP state. **Table S6.** Results of kinesin−tubulin binding free energy calculation for ADP, APO, and ATP state. **Table S7.** Results of partition of kinesin−tubulin binding free energy for ADP, APO, and ATP state. **Table S8**. Comparison of the tilt angles of central β-sheet with the results of ref 52. **Movie S1**. Combined snapshots of tubulin-binding interface during MD simulation in ADP, APO, and ATP state. **Movie S2.** Combined snapshots of nucleotide-binding pocket during MD simulation in ADP, APO, and ATP state. This material is available free of charge via the Internet at http://pubs.acs.org.

■ AUTHOR INFORMATION

Corresponding Author

*E-mail: wjzheng@buffalo.edu. Tel: (716) 6452947. Fax: (716) 6452507.

Funding

National Science Foundation (Grant #0952736).

Notes

The authors declare no competing financial interest.

■ ACKNOWLEDGMENTS

We thank Dr. Sindelar for sharing his cryo-EM maps for kinesin-decorated MT filaments.

■ ABBREVIATIONS

ADP, adenosine diphosphate; ATP, adenosine triphosphate; CCC, cross-correlation coefficient; CSA, contact surface area; EM, electron microscopy; HB, hydrogen bond; Pi, inorganic phosphate; MT, microtubule; MD, molecular dynamics; PCA, principal component analysis; PDB, Protein Data Bank; RMSD, root mean squared deviation; RMSF, root mean squared fluctuation

■ REFERENCES

(1) Hirokawa, N. (1998) Kinesin and dynein superfamily proteins and the mechanism of organelle transport. *Science 279*, 519−526.

(2) Tucker, C., and Goldstein, L. S. (1997) Probing the kinesin-microtubule interaction. *J. Biol. Chem. 272*, 9481−9488.

(3) Vale, R. D., Reese, T. S., and Sheetz, M. P. (1985) Identification of a novel force-generating protein, kinesin, involved in microtubule-based motility. *Cell 42*, 39−50.

(4) Vale, R. D., and Milligan, R. A. (2000) The way things move: looking under the hood of molecular motor proteins. *Science 288*, 88−95.

(5) Case, R. B., Rice, S., Hart, C. L., Ly, B., and Vale, R. D. (2000) Role of the kinesin neck linker and catalytic core in microtubule-based motility. *Curr. Biol. 10*, 157−160.

(6) Vale, R. D., Case, R., Sablin, E., Hart, C., and Fletterick, R. (2000) Searching for kinesin's mechanical amplifier. *Philos. Trans. R. Soc., B 355*, 449−457.

(7) Valentine, M. T., and Gilbert, S. P. (2007) To step or not to step? How biochemistry and mechanics influence processivity in Kinesin and Eg5. *Curr. Opin. Cell Biol. 19*, 75−81.

(8) Gilbert, S. P., Webb, M. R., Brune, M., and Johnson, K. A. (1995) Pathway of processive ATP hydrolysis by kinesin. *Nature 373*, 671−676.

(9) Ma, Y. Z., and Taylor, E. W. (1997) Kinetic mechanism of a monomeric kinesin construct. *J. Biol. Chem. 272*, 717−723.

(10) Moyer, M. L., Gilbert, S. P., and Johnson, K. A. (1998) Pathway of ATP hydrolysis by monomeric and dimeric kinesin. *Biochemistry 37*, 800−813.

(11) Cross, R. A. (2004) The kinetic mechanism of kinesin. *Trends Biochem. Sci. 29*, 301−309.

(12) Hackney, D. D. (1988) Kinesin ATPase: rate-limiting ADP release. *Proc. Natl. Acad. Sci. U. S. A. 85*, 6314−6318.

(13) Rice, S., Lin, A. W., Safer, D., Hart, C. L., Naber, N., Carragher, B. O., Cain, S. M., Pechatnikova, E., Wilson-Kubalek, E. M., Whittaker, M., Pate, E., Cooke, R., Taylor, E. W., Milligan, R. A., and Vale, R. D.

DOI: 10.1021/bi501056h
Biochemistry 2015, 54, 859−869

(1999) A structural change in the kinesin motor protein that drives motility. *Nature 402*, 778−784.
(14) Nitta, R., Kikkawa, M., Okada, Y., and Hirokawa, N. (2004) KIF1A alternately uses two loops to bind microtubules. *Science 305*, 678−683.
(15) Kikkawa, M., Sablin, E. P., Okada, Y., Yajima, H., Fletterick, R. J., and Hirokawa, N. (2001) Switch-based mechanism of kinesin motors. *Nature 411*, 439−445.
(16) Nitta, R., Okada, Y., and Hirokawa, N. (2008) Structural model for strain-dependent microtubule activation of Mg-ADP release from kinesin. *Nat. Struct. Mol. Biol. 15*, 1067−1075.
(17) Ma, Y. Z., and Taylor, E. W. (1995) Mechanism of microtubule kinesin ATPase. *Biochemistry 34*, 13242−13251.
(18) Gigant, B., Wang, W., Dreier, B., Jiang, Q., Pecqueur, L., Pluckthun, A., Wang, C., and Knossow, M. (2013) Structure of a kinesin−tubulin complex and implications for kinesin motility. *Nat. Struct. Mol. Biol. 20*, 1001−1007.
(19) Kikkawa, M., and Hirokawa, N. (2006) High-resolution cryo-EM maps show the nucleotide binding pocket of KIF1A in open and closed conformations. *EMBO J. 25*, 4187−4194.
(20) Hirose, K., Akimaru, E., Akiba, T., Endow, S. A., and Amos, L. A. (2006) Large conformational changes in a kinesin motor catalyzed by interaction with microtubules. *Mol. Cell 23*, 913−923.
(21) Sindelar, C. V., and Downing, K. H. (2007) The beginning of kinesin's force-generating cycle visualized at 9-A resolution. *J. Cell Biol. 177*, 377−385.
(22) Sindelar, C. V., and Downing, K. H. (2010) An atomic-level mechanism for activation of the kinesin molecular motors. *Proc. Natl. Acad. Sci. U. S. A. 107*, 4111−4116.
(23) Goulet, A., Behnke-Parks, W. M., Sindelar, C. V., Major, J., Rosenfeld, S. S., and Moores, C. A. (2012) The structural basis of force generation by the mitotic motor kinesin-5. *J. Biol. Chem. 287*, 44654−44666.
(24) Goulet, A., Major, J., Jun, Y., Gross, S. P., Rosenfeld, S. S., and Moores, C. A. (2014) Comprehensive structural model of the mechanochemical cycle of a mitotic motor highlights molecular adaptations in the kinesin family. *Proc. Natl. Acad. Sci. U. S. A. 111*, 1837−1842.
(25) Topf, M., Lasker, K., Webb, B., Wolfson, H., Chiu, W., and Sali, A. (2008) Protein structure fitting and refinement guided by cryo-EM density. *Structure 16*, 295−307.
(26) Jolley, C. C., Wells, S. A., Fromme, P., and Thorpe, M. F. (2008) Fitting low-resolution cryo-EM maps of proteins using constrained geometric simulations. *Biophys. J. 94*, 1613−1621.
(27) Velazquez-Muriel, J. A., Valle, M., Santamaria-Pang, A., Kakadiaris, I. A., and Carazo, J. M. (2006) Flexible fitting in 3D-EM guided by the structural variability of protein superfamilies. *Structure 14*, 1115−1126.
(28) Tan, R. K., Devkota, B., and Harvey, S. C. (2008) YUP.SCX: coaxing atomic models into medium resolution electron density maps. *J. Struct Biol. 163*, 163−174.
(29) Schroder, G. F., Brunger, A. T., and Levitt, M. (2007) Combining efficient conformational sampling with a deformable elastic network model facilitates structure refinement at low resolution. *Structure 15*, 1630−1641.
(30) Tama, F., Miyashita, O., and Brooks, C. L., 3rd (2004) Normal mode based flexible fitting of high-resolution structure into low-resolution experimental data from cryo-EM. *J. Struct Biol. 147*, 315−326.
(31) Suhre, K., Navaza, J., and Sanejouand, Y. H. (2006) NORMA: a tool for flexible fitting of high-resolution protein structures into low-resolution electron-microscopy-derived density maps. *Acta Crystallogr., Sect. D: Biol. Crystallogr. 62*, 1098−1100.
(32) Zheng, W. (2011) Accurate flexible fitting of high-resolution protein structures into cryo-electron microscopy maps using coarse-grained pseudo-energy minimization. *Biophys. J. 100*, 478−488.
(33) DiMaio, F., Tyka, M. D., Baker, M. L., Chiu, W., and Baker, D. (2009) Refinement of protein structures into low-resolution density maps using rosetta. *J. Mol. Biol. 392*, 181−190.
(34) Trabuco, L. G., Villa, E., Mitra, K., Frank, J., and Schulten, K. (2008) Flexible fitting of atomic structures into electron microscopy maps using molecular dynamics. *Structure 16*, 673−683.
(35) Trabuco, L. G., Villa, E., Schreiner, E., Harrison, C. B., and Schulten, K. (2009) Molecular dynamics flexible fitting: a practical guide to combine cryo-electron microscopy and X-ray crystallography. *Methods 49*, 174−180.
(36) Zheng, W., and Doniach, S. (2003) A comparative study of motor-protein motions by using a simple elastic-network model. *Proc. Natl. Acad. Sci. U. S. A. 100*, 13253−13258.
(37) Zheng, W., and Brooks, B. R. (2005) Normal-modes-based prediction of protein conformational changes guided by distance constraints. *Biophys. J. 88*, 3109−3117.
(38) Zheng, W., Brooks, B. R., and Hummer, G. (2007) Protein conformational transitions explored by mixed elastic network models. *Proteins 69*, 43−57.
(39) Zheng, W., and Tekpinar, M. (2009) Large-scale evaluation of dynamically important residues in proteins predicted by the perturbation analysis of a coarse-grained elastic model. *BMC Struct Biol. 9*, 45.
(40) Hyeon, C., and Onuchic, J. N. (2007) Mechanical control of the directional stepping dynamics of the kinesin motor. *Proc. Natl. Acad. Sci. U. S. A. 104*, 17382−17387.
(41) Zhang, Z., and Thirumalai, D. (2012) Dissecting the kinematics of the kinesin step. *Structure 20*, 628−640.
(42) Jana, B., Hyeon, C., and Onuchic, J. N. (2012) The origin of minus-end directionality and mechanochemistry of Ncd motors. *PLoS Comput. Biol. 8*, e1002783.
(43) Kanada, R., Kuwata, T., Kenzaki, H., and Takada, S. (2013) Structure-based molecular simulations reveal the enhancement of biased Brownian motions in single-headed kinesin. *PLoS Comput. Biol. 9*, e1002907.
(44) Karplus, M., and McCammon, J. A. (2002) Molecular dynamics simulations of biomolecules. *Nat. Struct. Biol. 9*, 646−652.
(45) Mackerell, A. D., Jr. (2004) Empirical force fields for biological macromolecules: overview and issues. *J. Comput. Chem. 25*, 1584−1604.
(46) Behnke-Parks, W. M., Vendome, J., Honig, B., Maliga, Z., Moores, C., and Rosenfeld, S. S. (2011) Loop L5 acts as a conformational latch in the mitotic kinesin Eg5. *J. Biol. Chem. 286*, 5242−5253.
(47) Zhang, W. (2011) Exploring the intermediate states of ADP-ATP exchange: a simulation study on Eg5. *J. Phys. Chem. B 115*, 784−795.
(48) Naber, N., Larson, A., Rice, S., Cooke, R., and Pate, E. (2011) Multiple conformations of the nucleotide site of Kinesin family motors in the triphosphate state. *J. Mol. Biol. 408*, 628−642.
(49) Hwang, W., Lang, M. J., and Karplus, M. (2008) Force generation in kinesin hinges on cover-neck bundle formation. *Structure 16*, 62−71.
(50) Harrington, T. D., Naber, N., Larson, A. G., Cooke, R., Rice, S. E., and Pate, E. (2011) Analysis of the interaction of the Eg5 Loop5 with the nucleotide site. *J. Theor. Biol. 289*, 107−115.
(51) Lakkaraju, S. K., and Hwang, W. (2011) Hysteresis-based mechanism for the directed motility of the Ncd motor. *Biophys. J. 101*, 1105−1113.
(52) Krukau, A., Knecht, V., and Lipowsky, R. (2014) Allosteric control of kinesin's motor domain by tubulin: a molecular dynamics study. *Phys. Chem. Chem. Phys. 16*, 6189−6198.
(53) Scarabelli, G., and Grant, B. J. (2013) Mapping the structural and dynamical features of kinesin motor domains. *PLoS Comput. Biol. 9*, e1003329.
(54) Aprodu, I., Soncini, M., and Redaelli, A. (2008) Interaction forces and interface properties of KIF1A kinesin-alphabeta tubulin complex assessed by molecular dynamics. *J. Biomech. 41*, 3196−3201.
(55) Li, M. H., and Zheng, W. J. (2011) Probing the Structural and Energetic Basis of Kinesin-Microtubule Binding Using Computational Alanine-Scanning Mutagenesis. *Biochemistry 50*, 8645−8655.

DOI: 10.1021/bi501056h
Biochemistry 2015, 54, 859−869

(56) Li, M., and Zheng, W. (2012) All-atom structural investigation of kinesin-microtubule complex constrained by high-quality cryo-electron-microscopy maps. *Biochemistry 51*, 5022−5032.
(57) Stone, J. E., Hardy, D. J., Ufimtsev, I. S., and Schulten, K. (2010) GPU-accelerated molecular modeling coming of age. *J. Mol. Graphics Modell. 29*, 116−125.
(58) Kull, F. J., Sablin, E. P., Lau, R., Fletterick, R. J., and Vale, R. D. (1996) Crystal structure of the kinesin motor domain reveals a structural similarity to myosin. *Nature 380*, 550−555.
(59) Eswar, N., Eramian, D., Webb, B., Shen, M. Y., and Sali, A. (2008) Protein structure modeling with MODELLER. *Methods Mol. Biol. 426*, 145−159.
(60) Parke, C. L., Wojcik, E. J., Kim, S., and Worthylake, D. K. (2010) ATP hydrolysis in Eg5 kinesin involves a catalytic two-water mechanism. *J. Biol. Chem. 285*, 5859−5867.
(61) Fiser, A., and Sali, A. (2003) ModLoop: automated modeling of loops in protein structures. *Bioinformatics 19*, 2500−2501.
(62) Pettersen, E. F., Goddard, T. D., Huang, C. C., Couch, G. S., Greenblatt, D. M., Meng, E. C., and Ferrin, T. E. (2004) UCSF chimera—A visualization system for exploratory research and analysis. *J. Comput. Chem. 25*, 1605−1612.
(63) Humphrey, W., Dalke, A., and Schulten, K. (1996) VMD: visual molecular dynamics. *J. Mol. Graphics 14* (33−38), 27−38.
(64) Phillips, J. C., Braun, R., Wang, W., Gumbart, J., Tajkhorshid, E., Villa, E., Chipot, C., Skeel, R. D., Kale, L., and Schulten, K. (2005) Scalable molecular dynamics with NAMD. *J. Comput. Chem. 26*, 1781−1802.
(65) MacKerell, A. D., Bashford, D., Bellott, M., Dunbrack, R. L., Evanseck, J. D., Field, M. J., Fischer, S., Gao, J., Guo, H., Ha, S., Joseph-McCarthy, D., Kuchnir, L., Kuczera, K., Lau, F. T. K., Mattos, C., Michnick, S., Ngo, T., Nguyen, D. T., Prodhom, B., Reiher, W. E., Roux, B., Schlenkrich, M., Smith, J. C., Stote, R., Straub, J., Watanabe, M., Wiorkiewicz-Kuczera, J., Yin, D., and Karplus, M. (1998) All-atom empirical potential for molecular modeling and dynamics studies of proteins. *J. Phys. Chem. B 102*, 3586−3616.
(66) Foloppe, N., and MacKerell, A. D. (2000) All-atom empirical force field for nucleic acids: I. Parameter optimization based on small molecule and condensed phase macromolecular target data. *J. Comput. Chem. 21*, 86−104.
(67) Deserno, M., and Holm, C. (1998) How to mesh up Ewald sums. I. A theoretical and numerical comparison of various particle mesh routines. *J. Chem. Phys. 109*, 7678−7693.
(68) Schlick, T., Skeel, R. D., Brunger, A. T., Kale, L. V., Board, J. A., Hermans, J., and Schulten, K. (1999) Algorithmic challenges in computational molecular biophysics. *J. Comput. Phys. 151*, 9−48.
(69) Brunger, A., Brooks, C. L., and Karplus, M. (1984) Stochastic boundary-conditions for molecular-dynamics simulations of St2 water. *Chem. Phys. Lett. 105*, 495−500.
(70) Martyna, G. J., Hughes, A., and Tuckerman, M. E. (1999) Molecular dynamics algorithms for path integrals at constant pressure. *J. Chem. Phys. 110*, 3275−3290.
(71) Eriksson, M. A., and Roux, B. (2002) Modeling the structure of agitoxin in complex with the Shaker K+ channel: a computational approach based on experimental distance restraints extracted from thermodynamic mutant cycles. *Biophys. J. 83*, 2595−2609.
(72) Gilson, M. K., and Honig, B. H. (1988) Energetics of charge-charge interactions in proteins. *Proteins 3*, 32−52.
(73) Im, W., Beglov, D., and Roux, B. (1998) Continuum Solvation Model: computation of electrostatic forces from numerical solutions to the Poisson−Boltzmann equation. *Comput. Phys. Commun. 111*, 59−75.
(74) Brooks, B. R., Brooks, C. L., 3rd, Mackerell, A. D., Jr., Nilsson, L., Petrella, R. J., Roux, B., Won, Y., Archontis, G., Bartels, C., Boresch, S., Caflisch, A., Caves, L., Cui, Q., Dinner, A. R., Feig, M., Fischer, S., Gao, J., Hodoscek, M., Im, W., Kuczera, K., Lazaridis, T., Ma, J., Ovchinnikov, V., Paci, E., Pastor, R. W., Post, C. B., Pu, J. Z., Schaefer, M., Tidor, B., Venable, R. M., Woodcock, H. L., Wu, X., Yang, W., York, D. M., and Karplus, M. (2009) CHARMM: the biomolecular simulation program. *J. Comput. Chem. 30*, 1545−1614.
(75) Muller, J., Marx, A., Sack, S., Song, Y. H., and Mandelkow, E. (1999) The structure of the nucleotide-binding site of kinesin. *Biol. Chem. 380*, 981−992.
(76) Hirokawa, N., Nitta, R., and Okada, Y. (2009) The mechanisms of kinesin motor motility: lessons from the monomeric motor KIF1A. *Nat. Rev. Mol. Cell Biol. 10*, 877−884.
(77) Kull, F. J., and Endow, S. A. (2013) Force generation by kinesin and myosin cytoskeletal motor proteins. *J. Cell Sci. 126*, 9−19.
(78) Sack, S., Kull, F. J., and Mandelkow, E. (1999) Motor proteins of the kinesin family. Structures, variations, and nucleotide binding sites. *Eur. J. Biochem. 262*, 1−11.
(79) Le Grand, S. M., and Merz, K. M. (1993) Rapid approximation to molecular surface area via the use of Boolean logic and look-up tables. *J. Comput. Chem. 14*, 349−352.
(80) Sosa, H., Peterman, E. J., Moerner, W. E., and Goldstein, L. S. (2001) ADP-induced rocking of the kinesin motor domain revealed by single-molecule fluorescence polarization microscopy. *Nat. Struct. Biol. 8*, 540−544.
(81) Song, Y. H., Marx, A., Muller, J., Woehlke, G., Schliwa, M., Krebs, A., Hoenger, A., and Mandelkow, E. (2001) Structure of a fast kinesin: implications for ATPase mechanism and interactions with microtubules. *EMBO J. 20*, 6213−6225.
(82) Chang, Q., Nitta, R., Inoue, S., and Hirokawa, N. (2013) Structural basis for the ATP-induced isomerization of kinesin. *J. Mol. Biol. 425*, 1869−1880.
(83) Rice, S. (2014) Structure of kif14: an engaging molecular motor. *J. Mol. Biol. 426*, 2993−2996.
(84) Arora, K., Talje, L., Asenjo, A. B., Andersen, P., Atchia, K., Joshi, M., Sosa, H., Allingham, J. S., and Kwok, B. H. (2014) KIF14 binds tightly to microtubules and adopts a rigor-like conformation. *J. Mol. Biol. 426*, 2997−3015.
(85) Grant, B. J., McCammon, J. A., Caves, L. S., and Cross, R. A. (2007) Multivariate analysis of conserved sequence-structure relationships in kinesins: coupling of the active site and a tubulin-binding subdomain. *J. Mol. Biol. 368*, 1231−1248.
(86) Li, M., and Zheng, W. (2013) All-atom molecular dynamics simulations of actin-myosin interactions: a comparative study of cardiac alpha myosin, beta myosin, and fast skeletal muscle myosin. *Biochemistry 52*, 8393−8405.
(87) Coureux, P. D., Wells, A. L., Menetrey, J., Yengo, C. M., Morris, C. A., Sweeney, H. L., and Houdusse, A. (2003) A structural state of the myosin V motor without bound nucleotide. *Nature 425*, 419−423.
(88) Reubold, T. F., Eschenburg, S., Becker, A., Kull, F. J., and Manstein, D. J. (2003) A structural model for actin-induced nucleotide release in myosin. *Nat. Struct. Biol. 10*, 826−830.
(89) Kaan, H. Y., Hackney, D. D., and Kozielski, F. (2011) The structure of the kinesin-1 motor-tail complex reveals the mechanism of autoinhibition. *Science 333*, 883−885.
(90) Zhao, Y. C., Kull, F. J., and Cochran, J. C. (2010) Modulation of the kinesin ATPase cycle by neck linker docking and microtubule binding. *J. Biol. Chem. 285*, 25213−25220.
(91) Yun, M., Zhang, X., Park, C. G., Park, H. W., and Endow, S. A. (2001) A structural pathway for activation of the kinesin motor ATPase. *EMBO J. 20*, 2611−2618.
(92) Kull, F. J., and Endow, S. A. (2002) Kinesin: switch I & II and the motor mechanism. *J. Cell Sci. 115*, 15−23.

DOI: 10.1021/bi501056h
Biochemistry 2015, 54, 859−869